



CHORUS

This is the accepted manuscript made available via CHORUS. The article has been published as:

Orbital-dependent band renormalization in WTe_2 revealed by angle-resolved photoemission spectroscopy

R. Matsumoto, T. Sugimoto, T. Mizokawa, N. L. Saini, M. Arita, R. Jha, R. Higashinaka, T. D. Matsuda, and Y. Aoki

Phys. Rev. B **98**, 205138 — Published 19 November 2018

DOI: [10.1103/PhysRevB.98.205138](https://doi.org/10.1103/PhysRevB.98.205138)

Orbital dependent band renormalization in WTe_2 revealed by angle-resolved photoemission spectroscopy

R. Matsumoto,¹ T. Sugimoto,¹ T. Mizokawa,¹ N. L. Saini,² M. Arita,³
R. Jha,⁴ R. Higashinaka,⁴ T. D. Matsuda,⁴ and Y. Aoki⁴

¹*Department of Applied Physics, Waseda University, Shinjuku, Tokyo 169-8555, Japan*

²*Department of Physics, University of Roma "La Sapienza", 00185 Roma, Italy*

³*Hiroshima Synchrotron Radiation Center, Hiroshima University, Higashi-hiroshima, Hiroshima 739-0046, Japan*

⁴*Department of Physics, Tokyo Metropolitan University, Hachioji 192-0397, Japan*

Effect of electronic correlation on WTe_2 has been investigated by means of angle-resolved photoemission spectroscopy (ARPES) and band structure calculation. In the ARPES results, the valence band top with Te 5p character reaches the Fermi level and forms complicated hole pockets around the zone center. In addition, two electron pockets are observed besides the hole pockets. The position of the electron pockets is inconsistent with the prediction of band calculation suggesting importance of electronic correlation in WTe_2 . The present analysis indicates the correlation effect is associated with the excitonic coupling between the W 5d electron and Te 5p hole bands.

I. Introduction

Various narrow gap semiconductors and semimetals possessing band structure with non-trivial topological number have been attracting great interest due to their spin textured surfaces states which can be applied for future spintronics devices [1-8]. In addition, coexistence of electron and hole carriers in the topological semimetals can provide dramatic transport properties such as nonsaturating magnetoresistance [9-16]. Among the semimetals with nonsaturating magnetoresistance, electronic structure of WTe_2 has been studied in details by means of angle-resolved photoemission spectroscopy (ARPES) and has been considered as a Weyl semimetal candidate [17-25]. The crystal structure and the corresponding first BZ of WTe_2 are shown in Figs. 1(a) and (b), respectively. Although layered transition-metal dichalcogenides generally exhibit trigonal crystal structure with triangular lattice layers of transition-metal ions, WTe_2 has orthorhombic distortion with formation of zig-zag chains of W ions. The zig-zag chain runs along the a-axis of the orthorhombic lattice.

In the pioneering work by Augustin *et al.*, it has been pointed out that the electronic states near the Fermi level are characterized by W 5d and Te 5p orbitals with strong

covalency. The W 5d t_{2g} bands (xy, yz, and zx orbitals) are split into bonding and antibonding bands due to strong W-W bond in the zig-zag chain. (Here, the x-, y-, and z-axes are along the a-, b-, and c-axis of the orthorhombic lattice.) The hole pockets around Γ point mainly have the Te 5p character while the Fermi surface around $0.2\Gamma X$ and the electron pocket around $0.6\Gamma X$ have substantial W 5d xy components. (The xy orbital in the present definition is denoted as $d_{x^2-y^2}$ and the ΓX is as ΓY in ref. 17). In a recent ARPES work, a pair of electron and hole pockets were reported along the Γ -X cut in the rectangular Brillouin zone by Pletikosić *et al* using photon energies of 21 eV and 38-78 eV [18]. The compensation of the electron and hole carriers is responsible for the nonsaturating magnetoresistance. In addition to the electron and hole pockets, a very steep band crosses or touches the Fermi level. Pletikosić *et al.* argued that the steep band is inconsistent with the band structure calculation by Ali *et al.* [15] and consistent with that by Augustin *et al* [17]. However, by means of Laser ARPES, Wu *et al.* revealed that the steep band also forms another hole pocket consistent with their band structure calculation [19] as well as that by Ali *et al* [15]. In addition, Jiang *et al.* showed that an additional hole pocket exists at Γ point and the electron pocket reported by Pletikosić *et al.* is split into two electron pockets on the basis of ARPES result at photon energy of 57 eV [20]. They concluded that the spin-orbit coupling plays a major role in WTe_2 and that the nonsaturating magnetoresistance is caused by suppression of the spin texture [20].

It is difficult to reconcile the three different ARPES results [18-20] by chemical potential shift alone. Jiang *et al.* pointed out that the number of Fermi surfaces is very sensitive to the atomic positions and the observed nine Fermi surfaces would be explained by calculation with certain atomic arrangement [20]. One possibility is that the WTe_2 crystal studied by Jiang *et al.* includes additional lattice distortions at surface. In addition, Das *et al.* pointed out that position of the electron pockets is inconsistent with the bulk band calculation and concluded that the spectral weight projected to the first Te-W-Te layer can reproduce the position of the electron pocket [21]. So far, the complexity of the ARPES results has been assigned to the various surface effects. However, the discrepancy on the position of the electron pockets has been reported in the transport measurement by Zhu *et al.* [22] indicating that the disagreement between ARPES and band calculation is derived from the bulk electronic properties. Wu *et al.* [23], Bruno *et al.* [24] and Feng *et al.* [25] have observed a spin-textured surface band (topologically trivial Fermi arc) between the electron and hole pockets using Laser ARPES and that the surface band depends on the type of surface (Type A or Type B). If the bulk electron and hole pockets are modified by electronic correlation, it may affect the spin texture of the surface bands between them.

Since the Fermi surfaces are constructed from the Te 5p and W 5d orbitals, it is possible that the electronic states with W 5d character have stronger correlation effect than those of Te 5p character and that the orbital dependent band renormalization provides deviation from

the band structure calculations. Indeed, the band dispersions near the Fermi level reported in the three ARPES works largely deviate from the band structure calculations which may not be explained by merely adjusting atomic position at surface. In this context, it is highly interesting and important to examine the band dispersion considering their orbital character and to reconsider the assignment of the Fermi surfaces.

In the present work, we report an ARPES study of WTe_2 using photon energies of 22-28 eV and band structure calculations in order to understand the multiband nature of the W 5d and Te 5p bands.

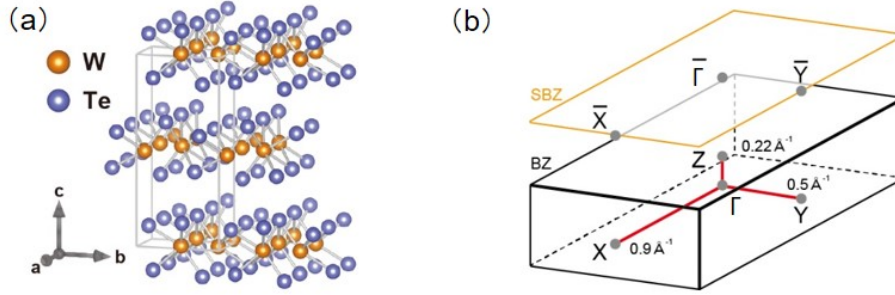


FIG. 1: (Color online) (a) Crystal structure of WTe_2 created by VESTA [10]. The blue and orange symbols represent Te and W atoms, respectively. (b) The first Brillouin zone of WTe_2 .

II. Experimental

High quality single crystals of WTe_2 were grown using Te flux method with W (99.99 %) and Te (99.999 %) by Aoki group at Tokyo Metropolitan University as reported in ref. 26 [26]. The lattice constants of $a = 3.4820 \text{ \AA}$, $b = 6.2603 \text{ \AA}$, and $c = 14.0326 \text{ \AA}$ were confirmed by x-ray diffraction in agreement with the reported values of $a=3.483 \text{ \AA}$, $b=6.265 \text{ \AA}$ and $c=14.043 \text{ \AA}$ [27,28]. The residual resistance ratio of the single crystals is about 1300-1330 [26] which is comparable to those in refs. 22, 29, and 30 [22,29,30] and higher than those in refs. 15, 20, 31 and 32 [15,20,31,32] depending on the growth technique [28]. ARPES measurements were performed at beamline 9A of Hiroshima Synchrotron Radiation Center (HiSOR). The base pressure of the spectrometer of HiSOR BL-9A was in the 10^{-9} Pa range. The layered single crystals with size of about $3\text{mm} \times 0.5\text{mm}$ were glued to sample holders using silver epoxy and cleaved by the top post method at 300 K under the ultrahigh vacuum. The single crystals were cleaved well and the size of $3\text{mm} \times 0.5\text{mm}$ was kept after the cleavage. The crystals were cooled to 20 K after the cleavage for the ARPES measurements. The ARPES data were obtained within 12 hours after the cleavage. The total energy resolution was set to about 15 meV for excitation energies of 22.9-27.9 eV in order to observe the valence band top near the zone center (Γ or Z point). Binding energies were

calibrated using the Fermi edge of gold reference samples. X-ray photoemission spectroscopy (XPS) was performed using JEOL9200 equipped with a Mg $K\alpha$ source. The total energy resolution was set to 1.0 eV. Band-structure calculations were performed using QUANTUM ESPRESSO 5.30 [33]. We have employed local density approximation with pseudopotentials of W.pz-spn-kjpaw_psl.1.0.0.UPF and Te.pz-dn-kjpaw_psl.0.2.2.UPF.

III. Results and Discussion

Figure 2 shows the core level XPS spectra of WTe_2 with characteristic Te 3d and W 4f core-level peaks. As shown in Fig. 2(a), the Te 3d core level is split into the Te 3d_{5/2} and 3d_{3/2} branches. The Te 3d_{5/2} peak has a tail on the higher binding energy side indicating correlation effect by the Te 5p conduction electrons. The W 4f core level is split into the W 4f_{7/2} and W 4f_{5/2} branches [Fig. 2(b)]. The asymmetry of the W 4f peaks is less apparent than that of the Te 3d peaks although the band structure calculations suggest that both Te 5p and W 5d states exist at the Fermi level.

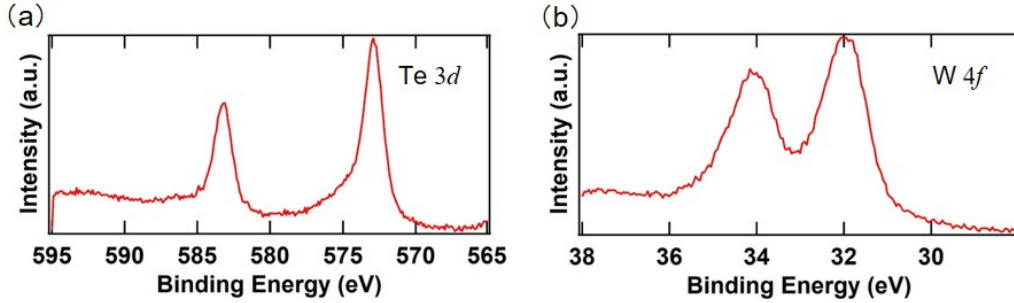


FIG. 2: (Color online) (a) Te 3d XPS spectrum of WTe_2 . (b) W 4f XPS spectrum of WTe_2 .

Figures 3(a)-(d) show ARPES data measured along the Γ -X direction with photon energies from 22.9 eV to 27.9 eV. In order to show the band dispersion more clearly, second derivative plots (with respect to energy) are displayed in Figs. 3(e)-(h) for the corresponding excitation energies. The overall band dispersions are roughly consistent with the previous ARPES work [17]. The dispersive bands between 2.0 eV and 2.5 eV can be assigned to Te 5p bands while the intense band around 1.5 eV has W 5d character. The hole bands with their maxima around 0.7 eV and 0.9 eV have W 5d yz and $3z^2-r^2$ characters, respectively. Near the Fermi level, the hole band with its maximum around 0.5 eV can be assigned to W 5d $3z^2-r^2$ and the hole band reaching the Fermi level is dominated by Te 5p.

Figure 4 shows ARPES data measured along the Γ -X direction with photon energies from 22.9 eV to 27.9 eV. In order to show the band dispersion, second derivative plots with respect to momentum are displayed in Figs. 4(a)-(d), and second derivative plots with respect to energy are displayed in Figs. 4(e)-(h) for the corresponding excitation energies.

At photon energies of 22.9 eV [Fig. 4(a)] and 23.8 eV [Fig. 4(b)], one hole pocket at the zone center and two electron pockets around $k_x \sim -0.3$ and 0.3 \AA^{-1} are observed as predicted by the calculation shown in Fig. 4(i). In the calculation, the electron pockets are located around $k_x \sim -0.4$ and 0.4 \AA^{-1} . Therefore, the observed position of the electron pockets is much closer to the Γ point than the calculated position. In the present results, the bottom of the electron bands is located at ~ 50 meV below the Fermi level whereas it is ~ 100 meV in the calculation suggesting that the electron band is shifted upwards by ~ 50 meV and the volume of the electron pockets is reduced from the theoretical value. Since the position of the electron pockets in the momentum space is modified from the band calculation probably due to the electronic correlation effect, it is difficult to apply a rigid band shift to the present system.

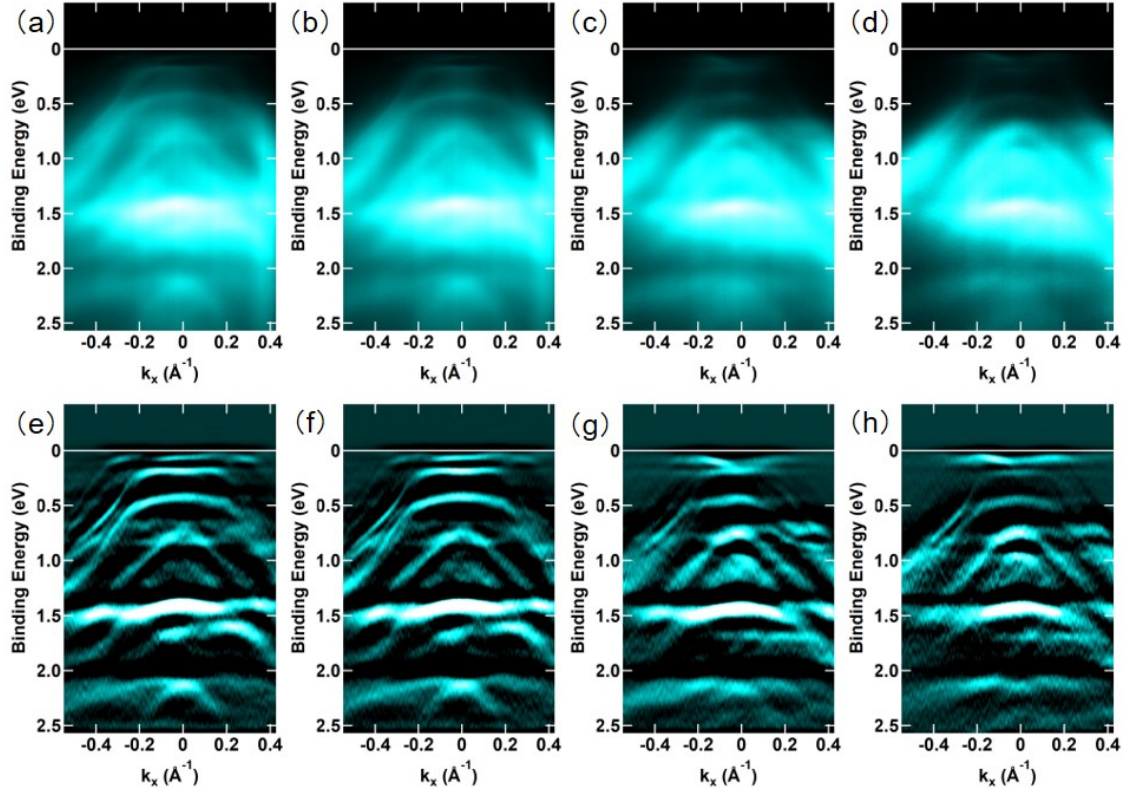


FIG. 3: (Color online) Wide range ARPES results. (a-d) ARPES intensity maps measured along the Γ -X direction at selected photon energies of (a) 22.9 eV, (b) 23.8 eV, (c) 25.9 eV, and (d) 27.9 eV. Second derivative (with respect to energy) maps along the Γ -X direction at selected photon energies of (e) 22.9 eV, (f) 23.8 eV, (g) 25.9 eV, and (h) 27.9 eV.

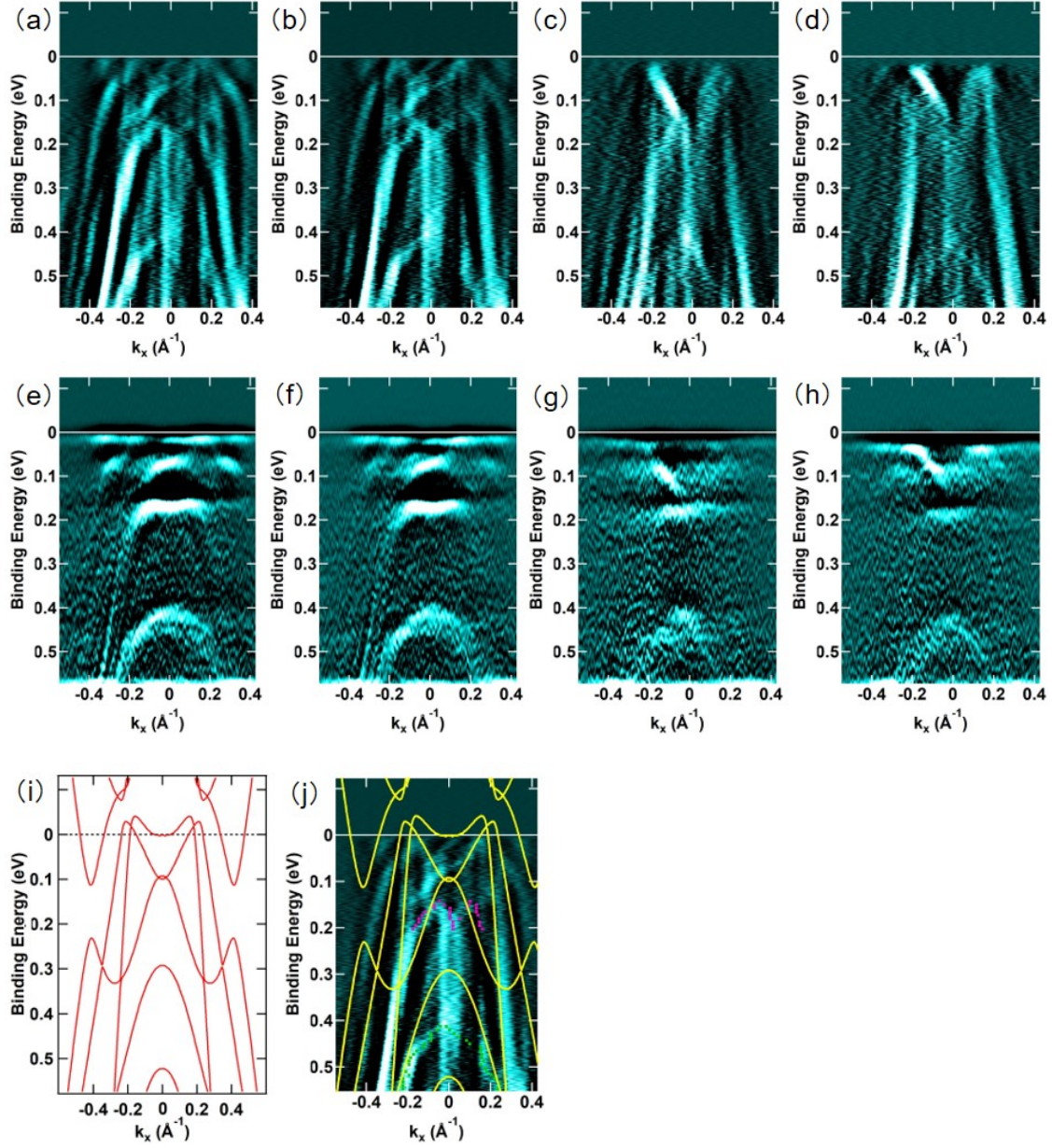


FIG. 4: (Color online) ARPES results and band calculations near the Fermi level. Second derivative (with respect to momentum) maps along the Γ -X direction at selected photon energies of (a) 22.9 eV, (b) 23.8 eV, (c) 25.9 eV, and (d) 27.9 eV. Second derivative (with respect to energy) maps along the Γ -X direction at selected photon energies of (e) 22.9 eV, (f) 23.8 eV, (g) 25.9 eV, and (h) 27.9 eV. (i) Band calculation for WTe_2 along the Γ -X direction. (j) Comparison between the calculation and the band map. The solid curves indicate calculated band dispersions. The small dots represent band positions determined from momentum distribution curves.

In addition to the electron and hole pockets, several holes bands are observed well below the Fermi level. A hole band is observed just below the electron pockets. This outer hole band is much closer to the Γ point than the calculated position [see Fig. 4(j)] consistent with the shift of the electron pockets. Also the energy gap between the electron band and the outer hole band is much smaller than the theoretical prediction. Another hole band with its maximum at ~ 100 meV below the Fermi level at the zone center is very flat compared to the calculation as shown in Figs. 4(e) and (f). The dispersion of the flat hole band changes in going from 22.9 eV to 27.9 eV [Figs. 4(g) and (h)]. The photon energy dependence of the hole band at ~ 100 meV excludes possibility of surface state. On the other hand, since the hole bands at ~ 200 and ~ 400 meV do not depend on the photon energies and have no counterparts in the calculation, they can be assigned to surface bands. As for the flat hole band at ~ 100 meV, the poor agreement between the experiment and theory can be assigned to correlation effect rather than the surface effect and would be consistent with the excitonic correlation between the electron and holes. One possible scenario is that the electron band with W 5d xy character (located around $\pm 0.5\Gamma_X$ in the calculation) is shifted upwards and the hole band with Te 5p character (located around Γ point) is shifted downwards due to excitonic correlation between the electron and hole bands.

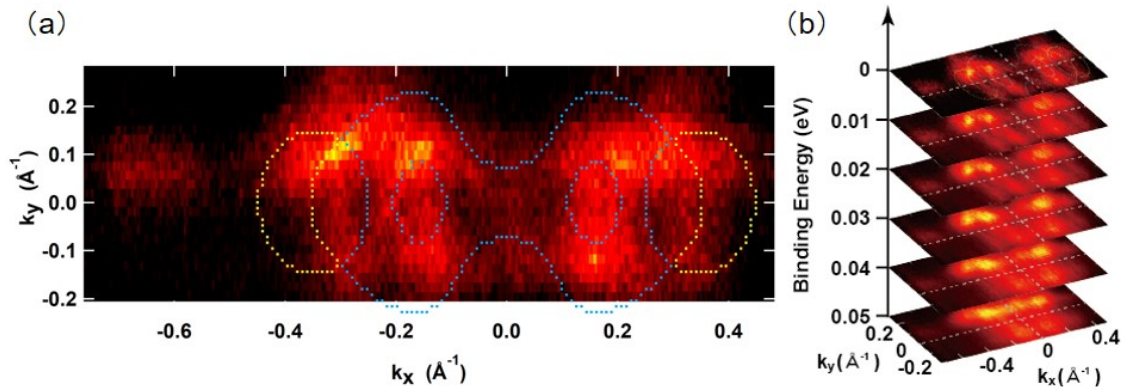


FIG. 5: (Color online) (a) The observed Fermi surfaces at 23.8 eV. The calculated electron and hole pockets are indicated by the yellow and blue dotted curves, respectively. (b) Constant energy maps at selected binding energies.

Figure 5(a) shows the Fermi surfaces observed at 23.8 eV. As shown in Fig. 5(b), as the binding energy increases, the hole pocket at the zone center becomes larger and the electron pocket at $k_x \sim -0.3 \text{ \AA}^{-1}$ becomes smaller, consistent with the interpretation for the band maps in Fig. 4. The electron pocket is crescent shaped in the calculation as shown in the dotted curves in Fig. 5(a). However, in the experiment, the position of the electron pockets becomes closer to the zone center than that predicted by the calculation as discussed in the previous paragraph. The electron pocket at $k_x \sim -0.3 \text{ \AA}^{-1}$ is partly consistent with the Laser ARPES

work by Bruno *et al.* [25]. In the present study, the electron pocket almost touches the hole pocket at $k_y \sim \pm 0.12 \text{ \AA}^{-1}$ which is different from the observation by Bruno *et al.* [25]. Since the photon energy dependence of the electron bands excludes the possibility of surface band, the present results indicate that the electron pocket is modified due to bulk electronic correlation. Considering the hole band at $\sim 100 \text{ meV}$ below the Fermi level, the electronic correlation is associated with the excitonic correlation between the Te 5p hole and W 5d electron. Such excitonic correlation effect would be important for understanding of the transport properties at bulk and surface of WTe_2 .

IV. Conclusion

In conclusion, we have studied the electronic structure of WTe_2 by means of angle-resolved photoemission spectroscopy and band structure calculation. The valence band top reaches the Fermi level and forms a complicated hole pocket around the zone center. In addition, two electron pockets are observed besides the hole pocket which are shifted towards the zone center compared to the band calculation. This observation is consistent with the transport study by Zhu *et al.* [22]. In addition, the electron band with W 5d xy character is shifted upwards while the hole band with Te 5p character is shifted down to $\sim 100 \text{ meV}$, indicating excitonic correlation between them.

Acknowledgements

This work was financially supported by JSPS KAKENHI (Grant No. JP15H03693, JP15H05884, JP16F16028 and JP16K05454) and by CREST-JST (Grant No. JPMJCR15Q2). The synchrotron radiation experiment was performed with the approval of HiSOR (16AG044).

References

- ¹ D. Hsieh, Y. Xia, L. Wray, D. Qian, A. Pal, J. H. Dil, J. Osterwalder, F. Meier, G. Bihlmayer, C. L. Kane, Y. S. Hor, R. J. Cava, and M. Z. Hasan, *Science* **323**, 919 (2009).
- ² D. Hsieh, Y. Xia, D. Qian, L. Wray, J. H. Dil, F. Meier, J. Osterwalder, L. Patthey, J. G. Checkelsky, N. P. Ong, A. V. Fedorov, H. Lin, A. Bansil, D. Grauer, Y. S. Hor, R. J. Cava, and M. Z. Hasan, *Nature* **460**, 1101 (2009).
- ³ C. Jozwiak, Y. L. Chen, A. V. Fedorov, J. G. Analytis, C. R. Rotundu, A. K. Schmid, J. D. Denlinger, Y.-D. Chuang, D.-H. Lee, I. R. Fisher, R. J. Birgeneau, Z.-X. Shen, Z. Hussain, and A. Lanzara, *Phys. Rev. B* **84**, 165113 (2011).
- ⁴ Z.-H. Pan, E. Vescovo, A. V. Fedorov, G. D. Gu, and T. Valla, *Phys. Rev. B* **88**, 041101(R) (2013).
- ⁵ B. Yan, B. Stadtmuller, N. Haag, S. Jakobs, J. Seidel, D. Jungkenn, S. Mathias, M. Cinchetti, M. Aeschlimann, and C. Felser, *Nat. Commun.* **6**, 10167 (2015).

- ⁶ Peng Zhang, J.-Z. Ma, Y. Ishida, L.-X. Zhao, Q.-N. Xu, B.-Q. Lv, K. Yaji, G.-F. Chen, H.-M. Weng, X. Dai, Z. Fang, X.-Q. Chen, L. Fu, T. Qian, H. Ding, and S. Shin, *Phys. Rev. Lett.* **118**, 046802 (2017).
- ⁷ B. Q. Lv, S. Muff, T. Qian, Z. D. Song, S. M. Nie, N. Xu, P. Richard, C. E. Matt, N. C. Plumb, L. X. Zhao, G. F. Chen, Z. Fang, X. Dai, J. H. Dil, J. Mesot, M. Shi, H. M. Weng, and H. Ding, *Phys. Rev. Lett.* **115**, 217601 (2015).
- ⁸ S.-Y. Xu, I. Belopolski, D. S. Sanchez, M. Neupane, G. Chang, K. Yaji, Z. Yuan, C. Zhang, K. Kuroda, G. Bian, C. Guo, H. Lu, T.-R. Chang, N. Alidoust, H. Zheng, C.-C. Lee, S.-M. Huang, C.-H. Hsu, H.-T. Jeng, A. Bansil, T. Neupert, F. Komori, T. Kondo, S. Shin, H. Lin, S. Jia, and M. Z. Hasan, *Phys. Rev. Lett.* **116**, 096801 (2016).
- ⁹ R. Xu, A. Husmann, T. F. Rosenbaum, M.-L. Saboungi, J. E. Enderby, and P. B. Littlewood, *Nature* **390**, 57 (1997).
- ¹⁰ M. Lee, T. F. Rosenbaum, M.-L. Saboungi, and H. S. Schnyders, *Phys. Rev. Lett.* **88**, 066602 (2002).
- ¹¹ F. Y. Yang, K. Liu, K. Hong, D. H. Reich, P. C. Searson, and C. L. Chien, *Science* **284**, 1335 (1999).
- ¹² F. Y. Yang, K. Liu, K. Hong, D. H. Reich, P. C. Searson, C. L. Chien, Y. Leprince-Wang, Kui Yu-Zhang, and K. Han, *Phys. Rev. B* **61**, 6631 (2000).
- ¹³ D.-X. Qu, Y. S. Hor, J. Xiong, R. J. Cava, and N. P. Ong, *Science* **329**, 821 (2010).
- ¹⁴ T. Liang, Q. Gibson, M. N. Ali, M. Liu, R. J. Cava, and N. P. Ong, *Nat. Mater.* **14**, 280 (2015).
- ¹⁵ M. N. Ali, J. Xiong, S. Flynn, J. Tao, Q. D. Gibson, L. M. Schoop, T. Liang, N. Haldolaarachchige, M. Hirschberger, N. P. Ong, and R. J. Cava, *Nature* **514**, 205 (2014).
- ¹⁶ K. Wang, D. Graf, L. Li, L. Wang, and C. Petrovic, *Sci. Rep.* **4**, 7328 (2014).
- ¹⁷ J. Augustin, V. Eyert, Th. Böker, W. Frentrup, H. Dwelk, C. Janowitz, and R. Manzke *Phys. Rev. B* **62**, 10812 (2000).
- ¹⁸ I. Pletikosić, Mazhar N. Ali, A. V. Fedorov, R. J. Cava, and T. Valla, *Phys. Rev. Lett.* **113**, 216601 (2014).
- ¹⁹ Y. Wu, N. H. Jo, M. Ochi, L. Huang, D. Mou, S. L. Bud'ko, P. C. Canfield, N. Trivedi, R. Arita, and A. Kaminski, *Phys. Rev. Lett.* **115**, 166602 (2015).
- ²⁰ J. Jiang, F. Tang, X. C. Pan, H. M. Liu, X. H. Niu, Y. X. Wang, D. F. Xu, H. F. Yang, B. P. Xie, F. Q. Song, P. Dudin, T. K. Kim, M. Hoesch, P. K. Das, I. Vobornik, X. G. Wan, and D. L. Feng, *Phys. Rev. Lett.* **115**, 166601 (2015).
- ²¹ P. K. Das, D. Di Sante, I. Vobornik, J. Fujii, T. Okuda, E. Bruyer, A. Gyenis, B. E. Feldman, J. Tao, R. Ciancio, G. Rossi, M. N. Ali, S. Picozzi, A. Yadzani, G. Panaccione, and R. J. Cava, *Nat. Commun.* **7**, 10847 (2016).
- ²² Z. Zhu, X. Lin, J. Liu, B. Fauqué, Q. Tao, C. Yang, Y. Shi, and K. Behnia, *Phys. Rev. Lett.* **114**, 176601 (2015).

- ²³ Yun Wu, Daixiang Mou, Na Hyun Jo, Kewei Sun, Lunan Huang, S. L. Bud'ko, P. C. Canfield, and Adam Kaminski, *Phys. Rev. B* **94**, 121113(R) (2016).
- ²⁴ F. Y. Bruno, A. Tamai, Q. S. Wu, I. Cucchi, C. Barreteau, A. de la Torre, S. McKeown Walker, S. Riccò, Z. Wang, T. K. Kim, M. Hoesch, M. Shi, N. C. Plumb, E. Giannini, A. A. Soluyanov, F. Baumberger, *Phys. Rev. B* **94**, 121112(R) (2016).
- ²⁵ Baojie Feng, Yang-Hao Chan, Ya Feng, Ro-Ya Liu, Mei-Yin Chou, Kenta Kuroda, Koichiro Yaji, Ayumi Harasawa, Paolo Moras, Alexei Barinov, Walid Malaeb, Cédric Bareille, Takeshi Kondo, Shik Shin, Fumio Komori, Tai-Chang Chiang, Youguo Shi, and Iwao Matsuda, *Phys. Rev. B* **94**, 195134 (2016).
- ²⁶ R. Jha, R. Higashinaka, T. D. Matsuda, R. A. Ribeiro, and Y. Aoki, *Physica B: Condensed Matter* **536**, 68 (2018).
- ²⁷ B. F. Mentzen and M. J. Sienko, *Inorg. Chem.* **15**, 2198 (1976).
- ²⁸ See Supplemental Materials in [URL] for powder x-ray diffraction analysis, typical size, and residual resistance ratio of the single crystals.
- ²⁹ Y. Luo, H. Li, Y.M. Dai, H. Miao, Y.G. Shi, H. Ding, A.J. Taylor, D.A. Yarotski, R.P. Prasankumar, J.D. Thompson, *Appl. Phys. Lett.* **107**, 182411 (2015).
- ³⁰ Y. Zhao, H. Liu, J. Yan, W. An, J. Liu, X. Zhang, H. Wang, Y. Liu, H. Jiang, Qing Li, Y. Wang, X.-Z. Li, D. Mandrus, X. C. Xie, M. Pan, and J. Wang, *Phys. Rev. B* **92**, 041104(R) (2015).
- ³¹ P. L. Cai, J. Hu, L. P. He, J. Pan, X. C. Hong, Z. Zhang, J. Zhang, J. Wei, Z. Q. Mao, and S. Y. Li, *Phys. Rev. Lett.* **115**, 057202 (2015).
- ³² D. Rhodes, S. Das, Q. R. Zhang, B. Zeng, N. R. Pradhan, N. Kikugawa, E. Manousakis, and L. Balicas, *Phys. Rev. B* **92**, 125152 (2015).
- ³³ <http://www.quantum-espresso.org/>